

Excitons in InP quantum dots

Huaxiang Fu and Alex Zunger

National Renewable Energy Laboratory, Golden, Colorado 80401

(Received 13 February 1998)

The excitonic spectrum of InP quantum dots is investigated using an atomistic pseudopotential approach for the single-particle problem and a state-dependent screened Coulomb interaction for the many-body problem. Our calculations show a different energy distribution of single-particle states relative to the commonly used $\mathbf{k}\cdot\mathbf{p}$ theory as well as significant parity mixing in the envelope functions, forbidden in 6×6 $\mathbf{k}\cdot\mathbf{p}$. The calculated excitonic spectrum, including seven excitons, explains well the recent experimental measurements. [S0163-1829(98)50424-9]

Colloidally prepared semiconductor quantum dots¹⁻³ have such a narrow size distribution and large confining potential that an unprecedented^{4,5} number of (as many as eight to ten) distinct electron-hole excitonic transitions have been observed in, e.g., CdSe,¹ InP,² and InAs (Ref. 3) dots of 20–60 Å diameters. Understanding the physical origin of these rich spectra in terms of the symmetry and envelope parity (i.e., s , p , d , ...) or the bulk parentage (light or heavy hole; Γ or L derived) of the single-particle electron and hole wave functions, and in terms of the nature^{6,7} of the *screened* many-body electron-hole Coulomb interactions is an outstanding challenge.¹⁻⁵ The traditional approach¹⁻³ to this problem is to use the $\mathbf{k}\cdot\mathbf{p}$ method in which the dot wave functions are expanded in terms of a small number of Γ -like *bulk* band-edge states, and to assume an average, state-independent Coulomb interaction with a constant bulk dielectric screening.⁶ Adjustment of the $\mathbf{k}\cdot\mathbf{p}$ parameters to the spectra of the quantum dots produces¹ a good fit for the three lowest of eight excitons in CdSe, but as recently shown² by Bertram *et al.* fails completely for excitons in InP. This failure is not related to surface states (which were removed via etching in the experimental procedure⁸), it represents a significant concern because the $\mathbf{k}\cdot\mathbf{p}$ method is the standard tool currently used to analyze the spectra of colloidal dots,¹⁻³ “self-assembled” dots,⁴ and other nanostructures.

In this paper we analyze the excitonic spectra of spherical InP colloidal dots using our recently developed *atomistic* approach^{9-11,7}—direct diagonalization of a pseudopotential Hamiltonian—and explain the physical identities of multiple excitonic transitions. This method was previously shown to correctly reproduce the size dependences of the band gaps¹⁰ and exchange splittings¹¹ in InP dots. Surprisingly, we find that, relative to the 6×6 $\mathbf{k}\cdot\mathbf{p}$, the atomistic theory produces for InP dots many more single-particle electron and hole states in the physically relevant energy range of ~ 1 eV from the dot’s conduction-band minimum (CBM) and valence-band maximum (VBM). Furthermore, we find that the atomistic single-particle states do not have purely odd or even angular-momentum envelope parity. Instead, strong parity mixing (permitted by the T_d point-group symmetry of zincblende dots) is apparent. In addition, some of the low-energy transitions in small dots are found to correspond to electron states that are not derived from the Brillouin-zone center (as assumed in all $\mathbf{k}\cdot\mathbf{p}$ models), but originate instead from zone-

edge (L point) states. Our atomistic approach, using state-dependent Coulomb interaction with position-dependent dielectric screening, is shown to be able to describe well the energies of the observed excitonic transitions.

We first solve the single-particle Schrödinger equation with Hamiltonian $H = -\frac{1}{2}\nabla^2 + \sum_{n,\alpha} v_\alpha(\mathbf{r}-\mathbf{R}_n)$, where v_α is the *screened* nonlocal pseudopotential of atom of type α located at position \mathbf{R}_n . This nonlocal pseudopotential includes spin-orbit interaction and has been derived¹⁰ by inverting the screened bulk potentials, which are computed self-consistently within the local-density approximation (LDA) for solid InP in a few crystal structures and volumes. The inverted potential was then adjusted to fit the *experimentally* observed bulk band structures while maintaining a large ($>99\%$) wave-function overlap with the LDA result. Since x-ray diffraction and transmission electron microscopy studies showed⁸ that the InP dots have a zinc-blende structure, being nearly spherical (slightly elliptic) with bulklike interatomic distance, and that the dot surfaces are passivated with organic ligand (emission due to surface states was eliminated via chemical etching), we have modeled the dots accordingly to simulate these conditions, i.e., we assume in the calculation spherical dots, and we passivate all surface dangling bonds by additional potentials.¹⁰ We find that as long as all surface states are removed from the band gap, the details of the passivation potential do not affect the results further.¹⁰ The dot wave functions are expanded in a set of plane-wave basis functions; the Hamiltonian is diagonalized using the folded spectrum method.⁹ Having obtained from $H\psi_i(\mathbf{r}) = \varepsilon_i\psi_i(\mathbf{r})$ the single-particle dot wave functions $\{\psi_i(\mathbf{r})\}$ and orbital energies $\{\varepsilon_i\}$, we calculate the two-particle excitonic transition energies $E_{ij} = (\varepsilon_j - \varepsilon_i) - J_{ij}$, where the screened Coulomb interaction energy between valence (v) and conduction (c) states is

$$J_{ij} = \int \frac{|\psi_{i,v}(\mathbf{r}_h)|^2 |\psi_{j,c}(\mathbf{r}_e)|^2}{\bar{\epsilon}(\mathbf{r}_h, \mathbf{r}_e) |\mathbf{r}_h - \mathbf{r}_e|} d\mathbf{r}_h d\mathbf{r}_e. \quad (1)$$

We assume that single-particle wave functions are unaltered by the electron-hole interactions. This was shown in Ref. 7 to be a good approximation for large dots. The screening $\bar{\epsilon}(\mathbf{r}_h, \mathbf{r}_e)$ includes both the electronic and ionic contributions,

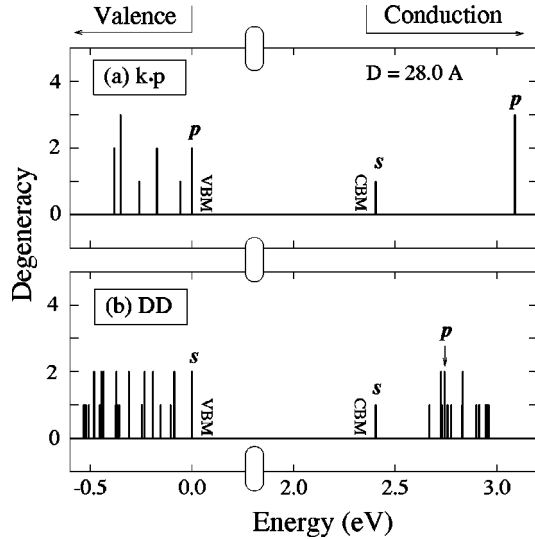


FIG. 1. The single-particle energy levels for a 28-Å, passivated InP dot as calculated by the direct diagonalization (DD) method and by the 6×6 $\mathbf{k} \cdot \mathbf{p}$ approach (with pseudopotential derived $\gamma_1 = 4.94$, $\gamma_2 = 1.79$, $\Delta_0 = 0.11$ eV). The VBM and CBM energies of the $\mathbf{k} \cdot \mathbf{p}$ calculation are aligned with those obtained by DD calculation. The degeneracy does not include the spin doublet. Note the very different energy-level separation in the two theories.

which are described using the modified Penn model¹² and the Haken formulas,¹³ respectively. The excitonic transition intensity is obtained by summing over the dipole matrix elements coupling hole state (i, v) and electron state (j, c), i.e.,

$$I(E) = \sum_{i,j} \frac{4e^2}{3m^2c^2} |\langle \psi_{i,v} | \mathbf{P} | \psi_{j,c} \rangle|^2 f(E - E_{ij}). \quad (2)$$

Here, $f(E - E_{ij})$ is a Gaussian broadening function. The single-particle pairs (i, j) contributing most to the peaks of $I(E)$ are identified. The bulk parentages of these single-particle states are then analyzed by projecting the relevant dot state ψ_i onto bulk states $\{\phi_{n\mathbf{k}}\}$ of band n and wave vector \mathbf{k} as

$$\psi_i^{\text{dot}}(\mathbf{r}) = \sum_{n\mathbf{k}} C_{n\mathbf{k}}^{(i)} \phi_{n\mathbf{k}}^{\text{bulk}}(\mathbf{r}) = \sum_{n\mathbf{k}} C_{n\mathbf{k}}^{(i)} [e^{i\mathbf{k} \cdot \mathbf{r}} u_{n\mathbf{k}}^{\text{bulk}}(\mathbf{r})]. \quad (3)$$

Once the projection coefficients $\{C_{n\mathbf{k}}^{(i)}\}$ are calculated, the contribution of dot state i from bulk states whose wave vectors \mathbf{k} lie within the shell $k \rightarrow k + \Delta k$ is defined as (“Brillouin-zone parentage”):

$$\rho_i(k \rightarrow k + \Delta k) = \sum_{k < |\mathbf{k}| < k + \Delta k} \sum_n |C_{n\mathbf{k}}^{(i)}|^2. \quad (4)$$

This identifies the region in the Brillouin zone (BZ) from which the dot orbits are constructed. The dot’s states are further analyzed by decomposing the microscopic wave functions $\{\psi_i\}$ into envelope functions with different angular momenta. This is accomplished by expanding the cell-periodic Bloch functions $u_{n\mathbf{k}}^{\text{bulk}}$ of Eq. (3) by a set of Γ -point-only Bloch functions $\{u_{n\Gamma}^{\text{bulk}}\}$, and by further expanding $e^{i\mathbf{k} \cdot \mathbf{r}}$ in spherical waves: $\psi_i^{\text{dot}}(\mathbf{r}) = \sum_n [\sum_{lm} f_{lm}^{(n)}(r) Y_{lm}(\theta, \varphi)] u_{n\Gamma}^{\text{bulk}}(\mathbf{r})$. The calculated microscopically derived envelope functions $\{f_{lm}^{(n)}(r)\}$ are used to identify the angular components making up the dot’s orbits. The angular contribution of a certain l is obtained by integrating the envelope functions squared inside the dot, i.e.,

$$\omega_l = \sum_n \sum_m \int r^2 |f_{lm}^{(n)}(r)|^2 dr. \quad (5)$$

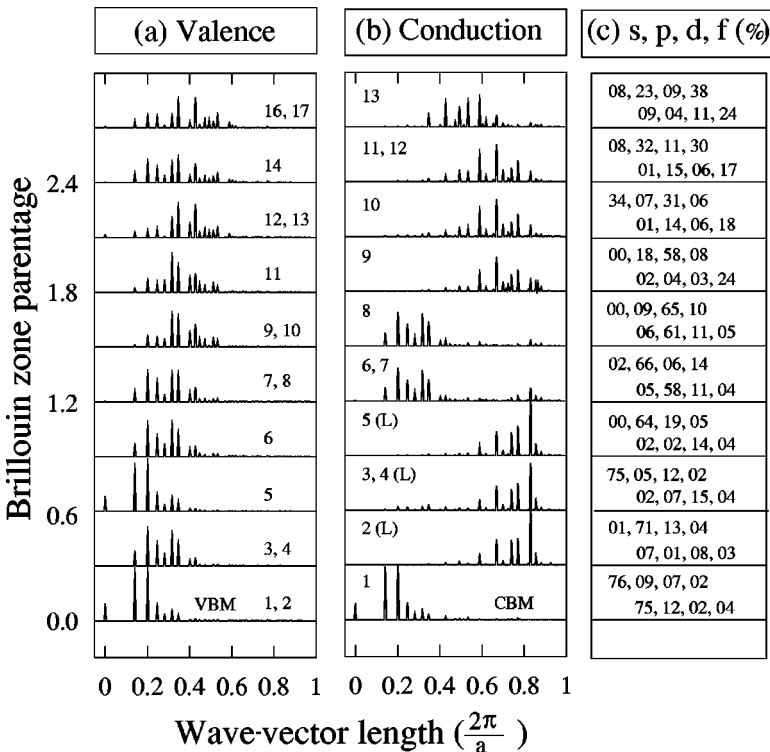


FIG. 2. The Brillouin-zone parentage [Eq. (4)] for (a) valence states; (b) conduction states of a 28-Å InP dot. The dot valence (conduction) states are numbered (without counting spin degeneracy) in decreasing (increasing) energy. The percentage of envelope angular-momentum components [Eq. (5)] for the states in (a) and (b) are given, respectively, in the first and second rows in part (c). The four numbers in each row represent in percentage the contributions of s , p , d , and f angular components from the lowest 16 (including spin) bulk bands, respectively.

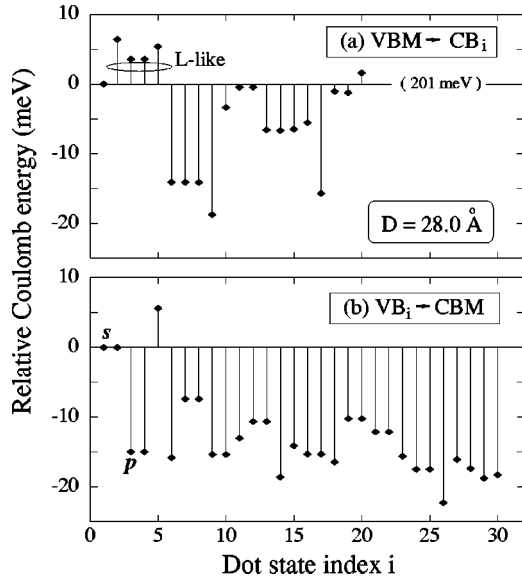


FIG. 3. Screened Coulomb interaction between (a) dot VBM and the lowest 20 conduction states; (b) dot CBM and the highest 30 valence states, for the InP dot of 28-Å diameter. In this figure, the Coulomb interaction between the VBM and the CBM (201 meV) is taken as reference.

Figure 1 shows the energy distribution of the single-particle valence and conduction states of a spherical $\text{In}_{240}\text{P}_{225}$ passivated dot (with diameter of 28 Å), as calculated by the present direct diagonalization (DD) and by the 6×6 $\mathbf{k} \cdot \mathbf{p}$ approach (in the latter case, we use pseudopotential-derived¹⁴ $\mathbf{k} \cdot \mathbf{p}$ parameters $\gamma_1 = 4.94$, $\gamma_2 = 1.79$, $\Delta_0 = 0.11$ eV). Surprisingly, we see that within the energy windows of ~ 0.5 eV from the VBM and ~ 0.5 eV from the CBM, the atomistic DD theory produces many more single-particle states, and thus different energy spacing relative to the 6×6 $\mathbf{k} \cdot \mathbf{p}$ theory. To understand the origin of these states, Fig. 2 analyzes the Brillouin-zone parentage [Eq. (4)] and the envelope-function angular-momentum character [Eq. (5)] of the single-particle states of the same dot, as obtained in the present atomistic approach. The valence (conduction) states

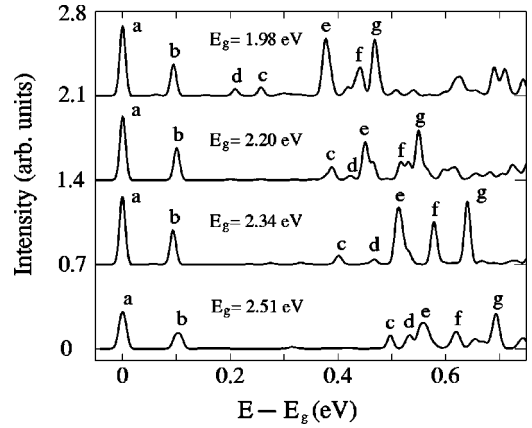


FIG. 4. Theoretical single-dot excitonic spectra [Eq. (2)] for four InP dots with diameters of 20.2, 23.7, 28.0, and 34.8 Å from the bottom to the top curves, respectively. The electron-hole Coulomb interactions are included. E_g is the excitonic band gap. The peaks assigned to the experimentally observed PLE peaks are labeled by letters *a* to *f*.

are numbered by $1, 2, \dots, N$ in decreasing (increasing) energy from the dot's VBM (CBM). Inspection of Fig. 2 shows that (i) while the dot's *low-energy* valence states are derived mostly from the vicinity of the $k=0$ Γ point, as the hole energy increases, the Brillouin-zone parentage progressively migrates away from Γ (i.e., peaks in Fig. 2 move to the right). (ii) The dot's *lowest* conduction state is Γ derived, but the next four states [numbered 2 to 5 in Fig. 2(b)] are *L* derived, and thus cannot be described via the $\mathbf{k} \cdot \mathbf{p}$. (iii) The conduction states numbered 6 to 8 are *p*-like states, split by spin-orbit coupling. The energy differences between *s*- (CBM) and *p*-like dot conduction states are 374, 456, 338, and 308 meV for diameter $D = 20.2, 23.7, 28.0,$ and 34.8 Å dots, respectively. (iv) There is significant even-odd parity mixing in the envelope functions [see Fig. 2(c)]. For example, the sixth dot valence state is 64% *p*, 19% *d*, and 5% *f*; the 15th dot valence state (not shown in Fig. 2) is 21% *s*, 9% *p*, 17% *d*, and 32% *f*. This parity mixing, permitted by the atomistic T_d point-group symmetry, is forbidden in the 6×6 $\mathbf{k} \cdot \mathbf{p}$.

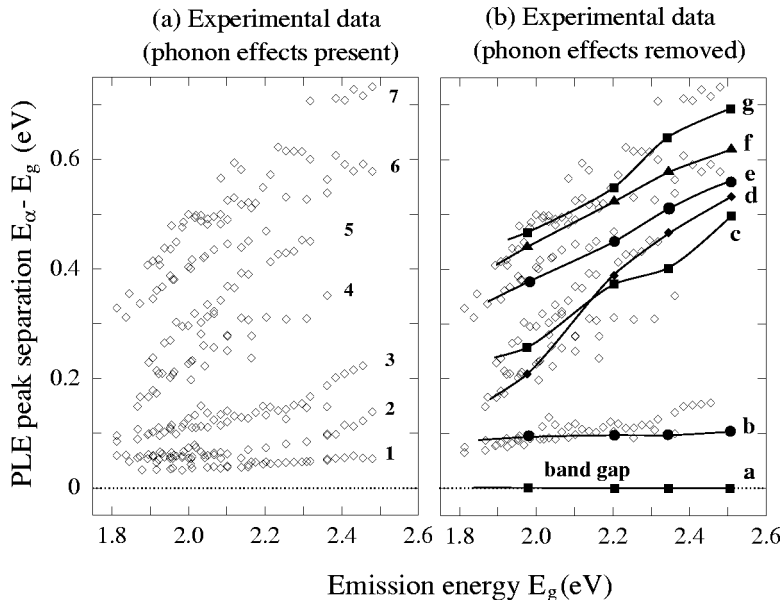


FIG. 5. Experimentally observed excitonic transition energies $E_a - E_g$ vs the excitonic band gap E_g : (a) with phonon effects present; (b) with phonon effects removed. In (b), the theoretical results are compared with experiment. Solid lines connecting the theoretical results are guides for the eyes.

The calculated screened electron-hole Coulomb interactions J_{ij} [Eq. (1)] between valence states i and conduction states j are shown in Fig. 3 for the InP dot of 28-Å diameter. All values are given with respect to $J_{\text{VBM,CBM}}$, which for this dot is calculated to be 201 meV. In previous calculations of the excitonic spectra,¹⁻³ J_{ij} were taken as constant for all (ij) pairs. The latter approach gives⁶ a much smaller value of 148 meV for the 28-Å dot. Interestingly, we see that the Coulomb interaction between the VBM hole and the L -like conduction states [in Fig. 3(a)] is the largest. Also, quite unexpectedly from the symmetry consideration, the dot valence states of s - and p -like symmetries [numbered 1 and 3 in Fig. 3(b)] have quite similar (only by a 7% difference) Coulomb interactions with the s -like dot CBM.

Having obtained the single-particle energies and the Coulomb interaction energies, Fig. 4 shows the calculated (with Coulomb interaction included) intensity $I(E)$ [Eq. (2)] for the transitions between valence and conduction states. The main peaks are assigned the letters a to g (in assigning the transitions we assume that it is possible to observe an *isolated* peak even if it is relatively weak).

Before comparing our transition energies with experiments, we note that our theory corresponds to a *nonvibrating* system and neglects exchange interactions.¹⁵ Figure 5(a) shows the experimental photoluminescence excitation (PLE) spectrum,² where the phonon and exchange effects are involved. We interpret¹⁶ the two lowest transitions in Fig. 5(a) as being phonon related: transition 1 is pure phonon band, while transition 2 originates from the process whereby the exciton is formed from a spin singlet state with simultaneous excitation of one phonon while the emission occurs from a spin triplet state. We thus remove the phonon effect by dropping from Fig. 5(a) transition 1 and by subtracting the phonon energy from transition 2. We further remove the exchange effect by subtracting the exchange splitting from both transitions 2 and 3. Higher energy transitions will not be affected significantly by phonon and exchange, and thus are kept unchanged. The ensuing experimental data with phonon and exchange effects removed are plotted in Fig. 5(b), and are compared with the theoretical results obtained from Fig. 4. We see that our atomistic calculation explains well the excitonic transition energies without invoking adjustable pa-

TABLE I. Analysis of the transition peaks a to g (see Fig. 4) in terms of valence-band (VB) and conduction-band (CB) single-particle states and their orbital characters, for an InP dot of 28-Å diameter. For a larger dot, the intensity of transition d (to L -like conduction states) is weak and peak d in the top curve of Fig. 4 results from the splitting of peak c .

Peak	VB index	Character	CB index	Character
a (gap)	1, 2	s	1	$s(\Gamma)$
b	5	s	1	$s(\Gamma)$
c	14; 16, 17	pf	1	$s(\Gamma)$
d	3, 4	p	3, 4, 5	(L)
e	3, 4	p	6, 7, 8	$p(\Gamma)$
f	6	p	6, 7, 8	$p(\Gamma)$
g	7, 8	p	6, 7	$p(\Gamma)$

rameters. Furthermore, we identify the microscopic origin of these transitions. Table I analyzes, for $D=28$ Å dot, the microscopic origins of peaks a to g in Fig. 5(b) in terms of the symmetry and bulk parentage of single-particle hole and electron states. Transition a ($s \rightarrow s$) is the band gap. Transition b results from the excitation from s -like spin-orbit split valence state to the s -like CBM. Curve b in Fig. 5(b) has almost a constant energy separation (~ 0.11 eV) from the fundamental band-gap transition (i.e., curve a). Transitions c and d involve valence states and conduction states with different angular components or bulk origins, thus being weak. Here, the valence states numbered 12 and 13 in Fig. 2, though being sd -like in the $\mathbf{k} \cdot \mathbf{p}$ language, are found to be nearly forbidden to the s -like CBM. Transitions e , f , and g in Fig. 5(b) occur between p -like valence states and p -like conduction states, and are strong.

In summary, a fully atomistic pseudopotential approach is used to calculate the excitonic transition spectrum in InP dots in a wide energy region, and more importantly, to analyze the microscopic origin of the transitions, explaining the surprising differences relative to the standard 6×6 $\mathbf{k} \cdot \mathbf{p}$ approach.

We thank D. Bertram and A. Nozik for discussing their data. This work was supported by the U.S. Department of Energy, OER-BES, under Grant No. DE-AC36-83CH10093.

¹D.J. Norris and M.G. Bawendi, Phys. Rev. B **53**, 16 338 (1996).

²D. Bertram, O.I. Micic, and A.J. Nozik, Phys. Rev. B **57**, R4265 (1998).

³U. Banin *et al.* (unpublished).

⁴M. Grundmann *et al.*, Phys. Rev. Lett. **74**, 3043 (1995).

⁵K.H. Schmidt *et al.*, Phys. Rev. B **54**, 11 346 (1996).

⁶L.E. Brus, J. Chem. Phys. **80**, 4403 (1984).

⁷A. Franceschetti and A. Zunger, Phys. Rev. Lett. **78**, 915 (1997).

⁸O.I. Micic *et al.*, Appl. Phys. Lett. **68**, 3150 (1996); O.I. Micic *et al.*, J. Phys. Chem. **98**, 4968 (1994).

⁹L.W. Wang and A. Zunger, J. Chem. Phys. **100**, 2394 (1994).

¹⁰H. Fu and A. Zunger, Phys. Rev. B **55**, 1642 (1997); **56**, 1496 (1997).

¹¹A. Zunger, MRS Bull. **23**, 35 (1998).

¹²D.R. Penn, Phys. Rev. **128**, 2093 (1962).

¹³H. Haken, Nuovo Cimento **10**, 1230 (1956).

¹⁴H. Fu, L.W. Wang, and A. Zunger, Phys. Rev. B **57**, 9971 (1998).

¹⁵A configuration-interaction calculation (Ref. 11) gives the excitonic *fine structure*, but will not be discussed here since the experiment deals with a wide and coarse energy scale.

¹⁶The phonon-assisted process separates in energy spacing the emission from the excitation source when the zero-phonon emission energy is close to the excitation energy.